IEICE Electronics Express, Vol.17, No.22, 1–6

LETTER

Bandpass filter with flat passband and transmission zeros using parallel-connected resistor loaded hairpin-shaped resonators

Tomohiro Tsukushi[1], **Satoshi Ono**[1, a)], **and Koji Wada**[1, b)]

Abstract A fourth-order flat passband bandpass filter (BPF) is realized using proposed resonators and half-wave open-looped resonators. The fourth-order flat passband BPF is necessary to prepare at least two kinds of resonators that have high and low unloaded quality factors. The proposed resonator is configured based on a half-wave hairpin-shaped resonator with a parallel-connected resistor. It is assigned as a resonator with a low unloaded quality factor. The advantage of the proposed resonator is flexible adjustment of the unloaded quality factor by changing the value and setting position of the resistor. Using equations and electromagnetic simulation, we show that the unloaded quality factor can be controlled by setting the position of the resistor. A half-wave open-looped resonator is assigned as a resonator with a high unloaded quality factor. Furthermore, a fourth-order flat passband BPF with transmission zeros and a flat passband is constructed on a printed circuit board by using the proposed resonators and half-wave open-looped resonators. Flat passband characteristics of a fourth-order BPF is satisfied with the design specifications.

Keywords: resistor-loaded half-wave hairpin-shaped resonator, half-wave open-looped resonator, bandpass filter (BPF), flat passband characteristics, transmission zero, coupling matrix

Classification: Microwave and millimeter-wave devices, circuits, and modules

1. Introduction

In wireless systems, frequency bands are assigned for many applications, including broadcast, communication and radar systems. It is necessary to employ bandpass filters (BPFs) with low insertion loss, sharp attenuation in the rejection band, and flatness for the passband since frequency resources are limited.

Superconducting filters [1, 2, 3] have excellent frequency characteristics that satisfy the need for low insertion loss, sharp skirt characteristics and a flat passband. However, superconducting filters are hard to employ as general electronic devices because a high-quality cryo-cooler is needed. Surface acoustic waveguide (SAW) filters [4, 5, 6, 7] have good frequency characteristics and are very compact. Therefore, SAW filters are employed in many of the present wireless systems. However, there is a limit to the operating frequency. Lacking proper candidates for RF BPFs with flat passband and sharp rejection performance is a problem for wireless systems, especially at higher operating frequencies. Although substrate integrated waveguide (SIW) filters [8, 9] are also good performance, the area of a resonator using SIW tends to be larger than a planar type.

Predistortion filter techniques [10, 11, 12] can realize flat passband and sharp rejection characteristics using normal metals. However, these techniques don't have good reflection characteristics. The non-uniform Q techniques [13, 14, 15, 16, 17] and resistive cross-coupling (RCC) techniques [17, 18, 19, 20] have better reflection characteristics than the predistortion technique. The former techniques need to control loss by using a resonator or by coupling loss between resonators. In other words, it is very important to flexibly control the unloaded quality factor. Basti et al. [17] showed a sixth-order flat passband BPF using a series-connected resistor loaded hairpin-shaped resonators. Although it is effective at realizing an unloaded quality factor of about 3 to 30, it is not possible to flexibly control the unloaded quality factor except by changing the element value of a resistor as shown in chapter 2. When a designer selects the structure of a resonator for BPF design, the unloaded quality factor of a resonator is almost uniquely determined because of the limitations of the circuit principle and structure. Moreover, if a multi-order flat passband BPF is configured in the future, it is more convenient than a multi-mode resonator to employ a single mode resonator for controlling the passband flatness and the out-of-band rejection characteristics.

In this paper, a novel resonator based on a single mode half-wave hairpin-shaped resonator is proposed. A fourth-order BPF with a flat passband characteristic using the proposed resonators and half-wave open loop resonators has been configured. The BPF was fabricated using a printed circuit board (PCB) and the frequency characteristics were measured.

2. Half-wave hairpin-shaped resonators loaded on a series- and parallel-connected resistor

Fig. 1 shows schematics and odd-mode equivalent circuits of a proposed resonator and a half-wave hairpin-shaped resonator with series-connected resistor [17]. Figs. 1 (a) and (b) are defined as parallel type and series type, respectively.

R, θ_1, and Z_0 show the resistance, the electrical length between R and the rounded part of the hairpin-shaped resonator, and the characteristic impedance of the transmission line, respectively. R is realized by using a chip resistor in

[1] The Graduate School of Informatics and Engineering, the University of Electro-Communications, 1-5-1 Chofugaoka, Chofu, Tokyo 182-8585, Japan

[a)] ono.satoshi@uec.ac.jp

[b)] wada.koji@uec.ac.jp

DOI: 10.1587/elex.17.20200320
Received September 24, 2020
Accepted October 7, 2020
Publicized October 19, 2020
Copyedited November 25, 2020

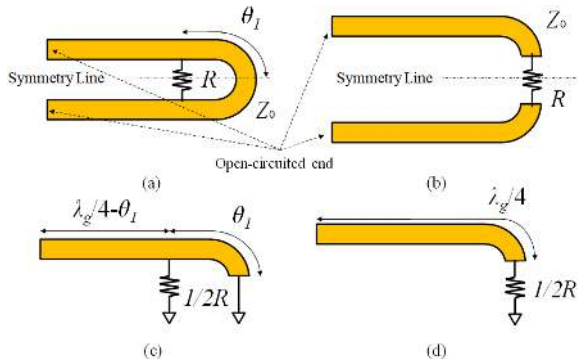

Fig. 1 (a) Schematic of proposed resonator (parallel type), (b) schematic of hairpin resonator with series-connected resistor [17] (series type), (c) odd-mode equivalent circuit of parallel type, (d) odd-mode equivalent circuit of series type.

this study. In Fig. 1 (b), a resistor is set to the position of the hairpin-shaped resonator with the strongest magnetic field for realizing low unloaded quality factor (Q_u). The strongest magnetic field is acquired at the center of the hairpin-shaped resonator because it is based on a $\lambda/2$ resonator with open-circuited ends.

The equations of Q_us with parallel- and series-connected Rs are shown as equations (1) and (2), respectively. Q_R means the unloaded quality factor due to R. Figs. 1 (c) and (d) are utilized for calculations of Q_us [21]. Magnetic store energy is considered when the equation (2) is introduced.

$$Q_u = \left(\frac{1}{Q_0} + \frac{1}{Q_R}\right)^{-1} = \left(\frac{1}{Q_0} + \frac{1}{\frac{\pi R}{8Z_0 \sin^2\theta_1}}\right)^{-1} = \left(\frac{1}{Q_0} + \frac{8Z_0 \sin^2\theta_1}{\pi R}\right)^{-1} \quad (\textit{Parallel type}), \tag{1}$$

$$Q_u = \left(\frac{1}{Q_0} + \frac{1}{Q_R}\right)^{-1} = \left(\frac{1}{Q_0} + \frac{1}{\frac{\pi Z_0}{2R}}\right)^{-1} = \left(\frac{1}{Q_0} + \frac{2R}{\pi Z_0}\right)^{-1} \quad (\textit{Series type}). \tag{2}$$

where Q_0, which is equal to 244.5, shows the original unloaded quality factor for only the hairpin-shaped resonator. The values of Rs are determined based on E24 series according to IEC publication 63. Figure 2 shows the contour of normalized Q_u for parallel type by Q_0 using equation (1). It is found that parallel type makes it possible to control wider than series type since there are two variables of θ_1 and R. Also, the solid line in Figure 3 (b) shows the normalized Q_u against θ_1 when R is equal to 1 kΩ. The results of normalized Q_u show an ability to change them from 0.03 to 0.995. The relationships between R and the normalized Q_u for parallel and series types are shown in Fig. 4. The results of normalized Q_u in the case of the parallel type show an ability to change them from 0.01 to 0.998, while those of the series type in Fig. 4 are limited to between 0.01 and 0.228. This means the parallel type is more flexible than the series type. Also, it has been confirmed that normalized Q_u for the

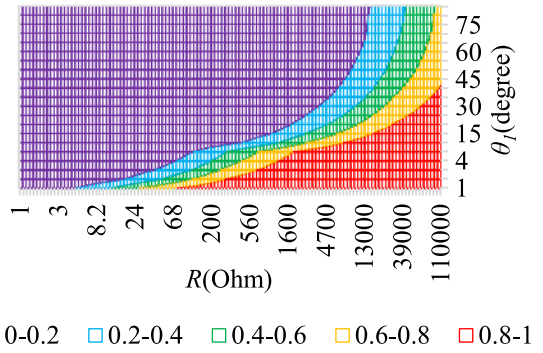

Fig. 2 The contour of normalized Q_u for parallel type by Q_0 using Eq. (1).

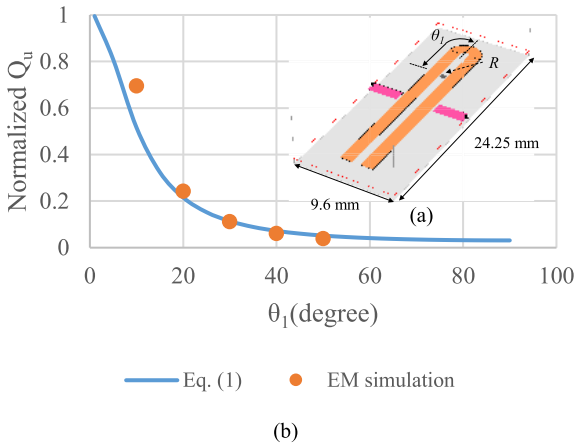

Fig. 3 (a) EM simulation model for parallel type, (b) comparison of calculation by Eq. (1) and EM simulation.

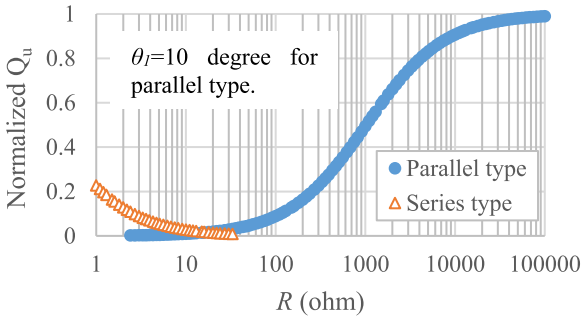

Fig. 4 Comparison of normalized Q_u for parallel and series types.

parallel type is able to change without almost changing resonant frequency f_r much at all by using a circuit simulator.

The calculated Q_u for parallel type using an electromagnetic (EM) simulator (Sonnet ver. 15.4) are shown in Fig. 3. Fig. 3 (a) shows the EM simulation model. Table I shows physical parameters of microstrip line model for the EM simulation. The entire length of the hairpin-shaped resonator is 20.25 mm in order to resonate at 2.4 GHz. The original unloaded quality factor Q_0 for only the hairpin-shaped resonator is equal to 266.5, which is determined by EM simulation. Z_0 and R are equal to 50 Ω and 1 kΩ, respectively. In Fig. 3 (b), the relationship between θ_1 and the calculated Q_u is shown. The Q_u using an EM simulator is calculated by dividing a resonant frequency of a resonator by the frequency width between two frequency points degrading 3 dB from the resonant frequency. The theoretical values are in good agreement with the results from EM simulation. This

Table I Physical parameters of a substrate for simulations.

Parameter	Value
Relative dielectric constant ε_r	3.2
$tan\delta$	0.001
Thickness of the dielectric substrate (mm)	0.5
Conductivity of conductor (S/m)	5.8×10^7
Thickness of conductor (μm)	18

is an important characteristic for the design of a flat passband BPF.

3. Coupling matrix for flat passband filter

Table II shows the design specifications for a flat passband BPF.

Table II Design specification.

Parameter	Value
Center frequency f_0 (GHz)	2.4
Passband bandwidth BW (MHz)	200
Fractional bandwidth FBW	0.083
Flatness	within 0.2 dB

Flatness is defined as the difference between the maximum and minimum of $|S_{21}|$ within the bandwidth (BW) of the specification. The coupling topology for a fourth-order flat passband BPF and the frequency characteristics of both a fourth-order flat passband BPF and a conventional one with transmission zeros are shown in Fig. 5. S, L and black circles mean the source, load and resonators of the BPF in Fig. 5 (a). The general Chebyshev function is assumed in order to generate the coupling topology. Although some have tried to configure flat passband BPFs with various kinds of coupling topologies, the coupling topology of Fig. 5 (a) is the best topology when it has an affinity between the structure design and the electrical circuit is considered. There is a unique feature for this coupling topology, namely, that it is divided into two sections for the high and low Q_u paths. The fourth-order flat passband BPF is synthesized after configuring the transfer functions for high and low Q_u paths. It is confirmed that high and low Q_u paths in the case of 150 and 40, respectively, have a flatter passband than simulated other results. The unloaded quality factor for the high Q_u path is determined to be 150 since that of a half-wave resonator is generally around 150, considering the physical parameters of PCB and the roughness of copper foil. In this paper, high and low Q_us are determined to be 150 and 40.

Equation (3) shows the immittance matrix [A] for the flat passband BPF. The values for matrix [A] are referred to [21]. The [A] is $(N+2) \times (N+2)$ matrix. N means the number of resonators.

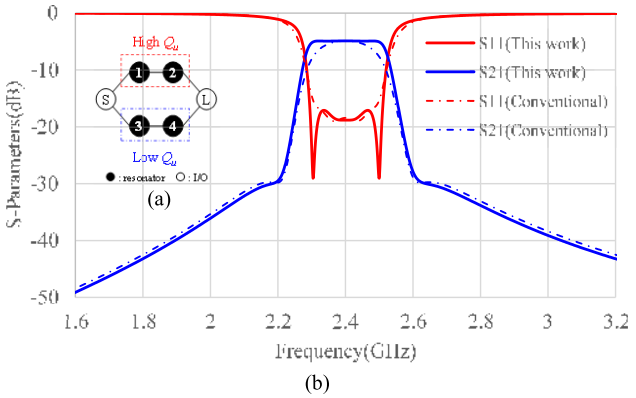

Fig. 5 (a) Coupling topology for flat passband BPF, (b) calculated frequency characteristics for conventional and flat passband fourth-order BPFs by coupling matrices.

$$
[A] = \begin{array}{c} \\ S \\ 1 \\ 2 \\ 3 \\ 4 \\ L \end{array}
\begin{array}{c}
\begin{array}{cccccc} S & 1 & 2 & 3 & 4 & L \end{array} \\
\begin{bmatrix}
-j & 0.5248 & 0 & 0.8788 & 0 & 0 \\
0.5248 & \Omega - j0.08 & 1.278 & 0 & 0 & 0 \\
0 & 1.278 & \Omega - j0.08 & 0 & 0 & 0.5248 \\
0.8788 & 0 & 0 & \Omega - j0.3 & -0.6904 & 0 \\
0 & 0 & 0 & -0.6904 & \Omega - j0.3 & 0.8788 \\
0 & 0 & 0.5248 & 0 & 0.8788 & -j
\end{bmatrix}
\end{array}, \tag{3}
$$

The relationship between [A] and coupling matrix [M] is shown as follows:

$$[A] = \Omega[U] - j[R] + [M], \tag{4}$$

$$\Omega = \frac{1}{FBW}\left(\frac{\omega}{\omega_0} - \frac{\omega_0}{\omega}\right), \tag{5}$$

where [U] and [R] show the identity matrix whose zero entries are the elements of U_{11} and $U_{(N+2),(N+2)}$ and a matrix whose only nonzero entries are the elements of R_{11} and $R_{(N+2),(N+2)}$. The detail information of immittance and coupling matrices are referred to [22, 23]. Equations (4)–(8) are needed for calculating the scattering parameters of the flat passband BPF.

$$S_{11}(\Omega) = 1 + 2j[A]^{-1}_{1,1}, \tag{6}$$

$$S_{21}(\Omega) = -2j[A]^{-1}_{6,1}, \tag{7}$$

$$\delta_i = \frac{BW}{f_0 \times Q_{ui}}. \tag{8}$$

External quality factor Q_e and coupling coefficient k_{ij} ($i, j = 1, 2, 3$ and 4), which are calculated based on Eq. (3), are shown in Table III. When the coupling matrix is denormalized, the value of FBW in Table II is used.

In Fig. 5 (b), the immittance matrix of Eq. (3) and the one of a conventional fourth-order BPF with transmission zeros are used. The conventional BPF is assumed to have a uniform Q (the unloaded quality factors of all resonators are the same), which is equal to 40.65. It is found that the edges of the frequency characteristics for the fourth-order flat passband BPF are not rounded. Also, sharp out-band rejection characteristics are maintained.

Table III External quality factors, coupling coefficients and f_r.

Parameter	Value
Q_{e13}=Q_{e2L}	43.6
Q_{eS3}=Q_{e4L}	15.5
k_{12}	0.1065
k_{34}	-0.0575
f_1=f_2=f_3=f_4(GHz)	2.4
Unloaded Quality factor of high Q_u path	150
Unloaded Quality factor of low Q_u path	40

4. Design of fourth-order BPF with flat passband

4.1 Design of the structures for high- and low-Q_u paths

Parallel types are employed in the case of composing a low-Q_u path. Figure 6 shows the structure of a low-Q_u path and the calculated results by an EM simulator and a coupling matrix. This structure is determined by comparing with the EM simulation in Fig. 6 and the calculated S-parameters using Eqs (3)–(8). The relative dielectric constant for configuring low- and high-Q_u paths and the fourth-order flat passband BPF was determined to be 3.23 after a preliminary experiment. Other parameters are the same as those in Table I. Resistor R and the setting position of R from the edge of the straight line are equal to 1 kΩ and 4 mm, respectively (θ_1 of Fig. 1 is equal to the electrical length of 24.8°). Resonant frequencies of both parallel types are 2.394 GHz. Those results near the resonant frequency are in good agreement, as shown in Fig. 6 (b). It is found that $|S_{21}|$ over the resonant frequency are degraded by the harmonic resonance.

The half-wave open-looped resonator is selected since the coupling coefficient between the 1st and 2nd resonators cannot be realized when the structure of a high-Q_u path is configured by hairpin-shaped resonators. Half-wave open-looped resonators are employed for composing a high-Q_u path. Figure 7 shows the structure of a high-Q_u path and the calculated results by an EM simulator and a coupling matrix. This structure is also determined by comparing with the EM simulation in Fig. 7 (a) and the calculated S-parameters using Eqs. (3)–(8). Resonant frequencies of both open-looped resonators are 2.4 GHz. It was found that $|S_{21}|$ under and over the resonant frequency are different from the calculated S-parameters by some cross-couplings among circuit patterns.

4.2 Design of fourth-order BPF with flat passband

Figure 8 shows the structure of a fourth-order flat passband BPF. Resistors of 1.0 × 0.5 mm in the BPF are selected film-type resistors (ERA2AEB102X, Panasonic Corporation) [24].

The high-frequency characteristics of the resistors are measured using a special fixture and the touchstone files are extracted. Input/output (I/O) feed lines for connecting low- and high-Q_u paths were configured by optimizing the length and characteristic impedance of the transmission lines, defined by Z_{High}, θ_{High}, Z_{low} and θ_{Low}. Z_{High}, θ_{High}, Z_{low} and θ_{Low} are equal to 54.4 Ω, 89.3°, 52.6 Ω and 87.9° at center

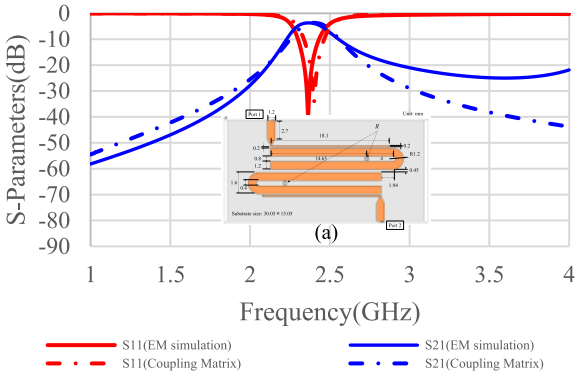

(b)

Fig. 6 (a) Structure of a low-Q_u path, (b) EM simulation results for Fig. 6 (a) and calculated S-parameters using Eqs. (3)–(8).

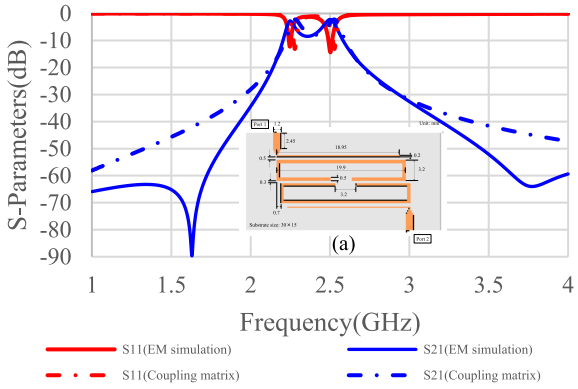

(b)

Fig. 7 (a) Structure of a high-Q_u path, (b) EM simulation results for Fig. 7 (a) and calculated S-parameters using Eqs. (3)–(8).

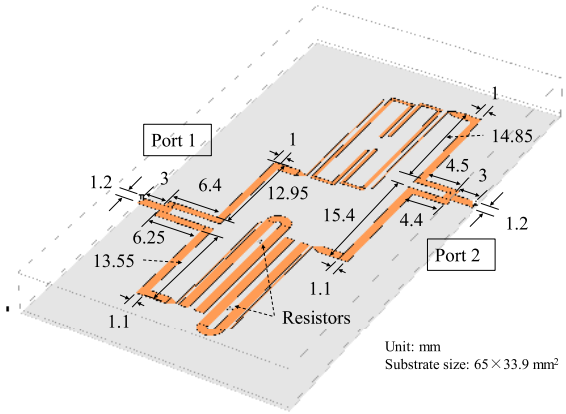

Fig. 8 Structure of fourth-order flat passband BPF.

frequency of BPF, respectively, after optimization using a circuit simulator. The detail information has been shown to [25]. The frequency characteristics of Fig. 8 are shown in the broken lines of Fig. 10 shown later. Those results satisfied the specifications.

5. Measurement of fourth-order BPF with flat passband

Figure 9 shows a photograph of the fabricated fourth-order flat passband BPF.

The substrate size is 65 mm × 33.9 mm. The guided

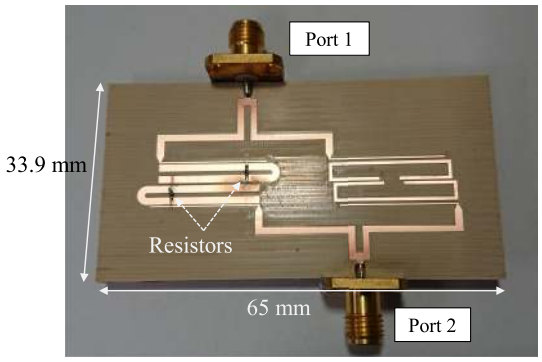

Fig. 9 Photograph of fabricated fourth-order flat passband BPF.

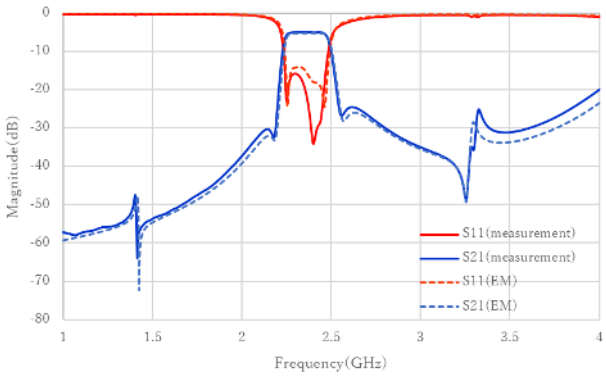

Fig. 10 EM simulated and measured results.

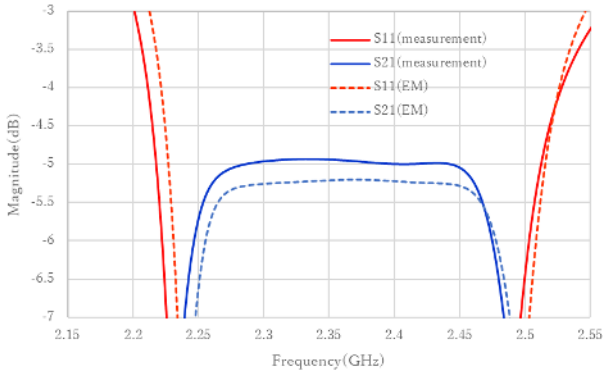

Fig. 11 Expansion of Fig. 10 around passband.

Table IV Simulated and measured results of fourth-order flat passband BPF.

Parameter	EM	Measurement
f_0 (GHz)	2.366	2.362
BW (MHz)	193	189
FBW	0.082	0.08
IL (dB)	5.2	4.93
Ripple (dB)	0.05	0.06
Flatness (dB)	< 0.2	< 0.2

wavelength λ_g, in the case of 50 Ω for the substrate is 78.1 mm. The normalized area of the fabricated fourth-order flat passband BPF is $0.832\lambda_g \times 0.434\lambda_g$. The measured results are shown in Figs. 10 and 11. Table IV shows the main parameters for the measured and simulated results. *IL*, *Ripple* and *Flatness* represent insertion loss, passband ripple and passband flatness, respectively. Although the center frequency shifts to the lower side at about 4 MHz, it is found that the measured S-parameters are in good agreement with those from EM simulation.

It is found that the advantages of the proposed BPF are flexibly controllable unloaded quality factor and good flatness in the passband compared with other references [14, 15, 16, 21, 26, 27, 28, 29, 30, 31, 32].

6. Conclusion

Parallel-connected resistor loaded half-wave hairpin-shaped resonator, which is defined parallel type, has been proposed. It is shown that the parallel type makes it possible to widely control the unloaded quality factor. A fourth-order BPF with flat passband characteristics and transmission zeros using the parallel type and half-wave open-loop resonators has been configured. This BPF is fabricated using a PCB and the frequency characteristics have been measured. The measurement results are in good agreement with those from simulation. This BPF has good flatness in the passband characteristics. Those characteristics were realized using the proposed resonator, which has a flexibly controllable unloaded quality factor.

Acknowledgments

This work is partly supported by the VLSI Design and Education Center (VDEC) at the University of Tokyo in collaboration with Keysight Technologies Japan, Ltd.

References

[1] C. Luo, *et al.*: "A wide stopband wideband HTS filter using stepped-impedance resonators with an interdigital capacitor structure," IEEE Trans. Appl. Supercond. **30** (2020) 1500305 (DOI: 10.1109/TASC.2019.2957164).
[2] N. Sekiya and T. Tsuruoka: "Improvement of filter properties of independently tunable superconducting dual-band bandpass filter," IEEE Trans. Appl. Supercond. **29** (2019) 1501004 (DOI: 10.1109/TASC.2019.2901708).
[3] D. Shojaeu-Asanjan and R.R. Mansour: "A novel low-temperature superconductor power limiter," IEEE Trans. Microw. Theory Techn. **67** (2019) 1005 (DOI: 10.1109/TMTT.2018.2883601).
[4] S. Fujii, *et al.*: "Diamond SAW resonator," 4th Australian Microwave Symposium (2020) (DOI: 10.1109/AMS48904.2020.9059368).
[5] O.L. Balysheva: "Problems of development of tunable SAW filters for mobile communication systems," Wave Electronics and its Application in Information and Telecommunication Systems (2020) (DOI: 10.1109/WECONF48837.2020.9131487).
[6] T. Takai, *et al.*: "High-performance SAW resonator with simplified $LiTaO_3/SiO_2$ double layer structure on Si substrate," IEEE Trans. Ultrason., Ferroelectr., Freq. Control **66** (2019) 1006 (DOI: 10.1109/TUFFC.2019.2898046).
[7] T. Kimura, *et al.*: "Comparative study of acoustic wave devices using thin piezoelectric plates in the 3–5-GHz range," IEEE Trans. Microw. Theory Techn. **67** (2019) 915 (DOI: 10.1109/TMTT.2018.2890661).
[8] R. Qin, *et al.*: "Duel-band filter with high out-of-band rejection using ACSRR-SIW technology," IEICE Electron. Express **12** (2020) (DOI: https://doi.org/10.1587/elex.17.20190743).
[9] X.-B. Ji, *et al.*: "A quasi-elliptic response triple-mode SIW bandpass filter with controllable transmission zeros," IEICE Electron. Express **16** (2019) 1 (DOI: https://doi.org/10.1587/elex.16.20190541).
[10] R.M. Livingston: "Predistorted waveguide filters for use in commu-

nications systems," IEEE G-MTT Int. Microw. Symp. Dig. (1969) 291 (DOI: 10.1109/GMTT.1969.1122705).
[11] A.E. Williams, *et al.*: "Predistortion techniques for multicoupled resonator filters," IEEE MTT-S Int. Microw. Symp. Dig. (1984) 290 (DOI: 10.1109/MWSYM.1984.1131768).
[12] M. Yu, *et al.*: "Novel adaptive predistortion technique for cross coupled filters," IEEE MTT-S Int. Microw. Symp. Dig. (2003) 7677298 (DOI: 10.1109/MWSYM.2003.1212521).
[13] J. Rao, *et al.*: "C-band microstrip lossy filter using resistive-loaded closed-loop resonators," Proc. 49th European Microwave Conference (2019) 360 (DOI: 10.23919/EuMC.2019.8910784).
[14] H. Guo, *et al.*: "Varactor-tuned dual-mode bandpass filter with nonuniform Q distribution," IEEE Microw. Wireless Compon. Lett. **28** (2018) 1002 (DOI: 10.1109/LMWC.2018.2870934).
[15] A.C. Guyette, *et al.*: "The design of microwave bandpass filters using resonators with nonuniform Q," IEEE Trans. Microw. Theory Techn. **54** (2006) 3914 (DOI: 10.1109/TMTT.2006.884627).
[16] C.-M. Tsai and H.-M. Lee: "The effects of component Q distribution on microwave filters," IEEE Trans. Microw. Theory Techn. **54** (2006) 1545 (DOI: 10.1109/TMTT.2006.871929).
[17] A. Basti, *et al.*: "Design of microstrip lossy filters for receivers in satellite transponders," IEEE Trans. Microw. Theory Techn. **62** (2014) 2014 (DOI: 10.1109/TMTT.2014.2337285).
[18] R. Das, *et al.*: "All passive realization of lossy coupling matrices using resistive decomposition technique," IEEE Access **7** (2018) 5095 (DOI: 10.1109/ACCESS.2018.2887298).
[19] L.-F. Qiu, *et al.*: "Substrate integrated waveguide filter with flat passband based on complex couplings," IEEE Microw. Wireless Compon. Lett. **28** (2018) 494 (DOI: 10.1109/LMWC.2018.2829349).
[20] J. Mateu, *et al.*: "Synthesis of 4th order lossy filters with uniform Q distribution," IEEE MTT-S Int. Microw. Symp. Dig. (2010) 568 (DOI: 10.1109/MWSYM.2010.5517741).
[21] L.-F. Qiu, *et al.*: "A flat-passband microstrip filter with nonuniform-Q dual-mode resonators," IEEE Microw. Wireless Compon. Lett. **26** (2016) 183 (DOI: 10.1109/LMWC.2016.2525017).
[22] R.K. Mongia, *et al.*: *RF and Microwave Coupled-Line Circuits* (Artech House, Boston, 2007).
[23] R.J. Cameron, *et al.*: *Microwave Filters for Communication Systems: Fundamentals, Design and Applications* (Wiley, New York, 2007) (DOI: 10.1002/9781119292371).
[24] Panasonic Corporation: Datesheet of metal film (thin film) chip resistors, high reliability type (2019) https://industrial.panasonic.com/cdbs/www-data/pdf/RDM0000/AOA0000C307.pdf
[25] T. Tsukushi, *et al.*: "Realization of flat passband characteristics for BPF using resistor loaded hairpin shaped resonators," IEICE Technical Report MW2018-109 (2018) 89.
[26] L.-F. Qiu, *et al.*: "Hybrid non-uniform-Q lossy filters with substrate integrated waveguide and microstrip resonators," IET Microw. Antenna P. **12** (2018) 92 (DOI: 10.1049/iet-map.2017.0060).
[27] F.J. Chen, *et al.*: "A lossy triple-mode microstrip filter with flat passband based on nonuniform Q-factors," Proc. Asia Pacific Microwave Conference (2014) 1139.
[28] J. Ni, *et al.*: "Design of microstrip lossy filter using an extended doublet topology," IEEE Microw. Wireless Compon. Lett. **24** (2014) 318 (DOI: 10.1109/LMWC.2014.2309089).
[29] M. Meng, *et al.*: "The design of parallel connected filter networks with nonuniform Q resonators," IEEE Trans. Microw. Theory Techn. **61** (2013) 372 (DOI: 10.1109/TMTT.2012.2230021).
[30] Q. Wu, *et al.*: "Design of microwave lossy filter based on hybrid structure," Proc. Int. Asia-Pacific Microwave Conference (2015) (DOI: 10.1109/apmc.2015.7412970).
[31] A. Périgaud, *et al.*: "Design of a hybrid SIW — microstrip lossy filter in LTCC technology," IEEE MTT-S International Microwave Workshop Series on Advanced Materials and Processes (IMWS-AMP 2017) (2017) (DOI: 10.1109/IMWS-AMP.2017.8247385).
[32] L.-F. Qiu, *et al.*: "A flat-passband filter with hybrid structure of substrate integrated waveguide and microstrip resonators based on predistorted nonuniform-Q method," Proc. Int. Asia-Pacific Microwave Conference (2018) (DOI: 10.23919/APMC.2018.8617474).